Pb-free solders for joint developments between YBCO tapes

Nooshin Goodarzi, Kévin Berger, Alexander Molodyk, Mark Ainslie, Tayebeh Mousavi

Journal of Superconductivity and Novel Magnetism (2026) 39:80
https://doi.org/10.1007/s10948-026-07159-y

RESEARCH

Pb-free Solders for Joint Developments Between YBCO Tapes

Nooshin Goodarzi[1] · Kévin Berger[2] · Alexander Molodyk[3] · Mark Ainslie[1] · Tayebeh Mousavi[1]

Received: 5 December 2025 / Accepted: 5 March 2026

Abstract

The development of Pb-free solder joints for ReBCO-coated conductors is essential for superconducting magnet manufacturers, who often rely on the Pb-Sn solders that will soon be restricted. This work investigates four low-melting Pb-free eutectic alloys, $In_{52}Sn_{48}$, $In_{66}Bi_{34}$, $Sn_{42}Bi_{58}$, and the ternary $In_{50}Sn_{15}Bi_{35}$, for fabricating lap joints between $YBa_2Cu_3O_{7-x}$ (YBCO) tapes. The electrical and mechanical properties, along with the microstructure of the joints, were characterized to identify the optimal Pb-free solder for enhanced electrical and mechanical performance. The choice of solder composition was found to control the microstructure of the solder area and the interface between the tape and the solder, having a substantial impact on the joint's final performance. Binary eutectic solder joints produced two-phase solder microstructures and thin interfacial intermetallic layers, yielding lower electrical resistance than the ternary eutectic InSnBi alloy, whose three-phase eutectic matrix ($\gamma+\beta+BiIn_2$) increases electron scattering and raises joint resistance. Among the evaluated candidates, the eutectic InBi solder exhibited the best overall performance, combining a uniform microstructure, the lowest joint resistance, and good mechanical strength, positioning it as a promising Pb-free alternative to conventional Pb-Sn solders for superconducting applications. All joints failed outside the solder region during tensile testing at room temperature, indicating that the fabricated solder joints exceeded the mechanical robustness of the original tape. These findings demonstrate that carefully selected Pb-free eutectic solders can produce reliable, low-resistance, and mechanically strong joints suitable for high-field superconducting magnet applications.

Keywords ReBCO-coated conductors · Pb-free eutectic alloys · Lap joints · Electrical and mechanical performance

1 Introduction

ReBCO-coated conductors are playing an increasingly vital role in the development of next-generation high-field magnets, power devices, and superconducting cables, due to their high critical current density and mechanical robustness under strong magnetic fields [1, 2]. However, for constructing practical devices, individual ReBCO tapes must be interconnected via joints. In fusion magnets, for instance, joints between ReBCO tapes are an essential part of superconducting magnet development. The electrical and mechanical performance of these joints strongly influences overall device efficiency and reliability [1, 3]. Soldering is the main non-superconducting joint technique widely used for ReBCO tapes due to the simple, reliable, and quick fabrication method, the relatively low joint resistance (R_j) obtained, the lack of extra structures required to maintain mechanical integrity under pressure, and its reasonable cost, satisfying the requirements of many applications [1, 3–6]. Moreover, this technique is adaptable for on-site fabrication [7] and is already well-established in the industry for large-scale applications [3].

The resistance and mechanical/electromechanical behavior of the soldered joints are affected by different factors, including the tape structure, joint geometry, type of solder material, solder layer thickness, and joining parameters, including soldering temperature and applied pressure during the soldering process [8, 9]. Hence, the choice of solder material is one of the main contributors affecting the overall performance of soldered joints [3, 10–12]. The solder type for joining YBCO tapes has been widely investigated

✉ Nooshin Goodarzi
nooshin.goodarzi@kcl.ac.uk

[1] Department of Engineering, King's College London, London WC2R 2LS, UK

[2] Université de Lorraine, GREEN, Nancy F-54000, France

[3] Faraday Factory Japan LLC, Tokyo, Japan

Published online: 22 April 2026

in the literature [3, 4, 13–15]. $Pb_{38}Sn_{62}$, as the eutectic composition of the Pb-Sn system with a melting point of 183 °C, has been commonly used to join ReBCO tapes and has the lowest resistivity amongst the solders at 77 K [3], demonstrating acceptable joint resistances in superconducting applications [13, 14]. However, the use of Pb will soon become restricted [3, 4, 15, 16], necessitating the development of alternative Pb-free solders for magnet applications that must fulfil the requirements for reliable operations [17, 18]. These requirements include low melting temperature, satisfactory wettability, and suitable thermal, electrical, and mechanical properties [10, 16]. The solder liquidus temperature should be sufficiently high to prevent melting of the joint during a quenching, but low enough to avoid overheating and delamination of the ReBCO layer, and degradation of its superconducting properties due to oxygen loss during joint fabrication [3, 4, 10]. Thus, low-temperature solders are advantageous, as they reduce the risk of damage to the delicate ReBCO structure while enabling the formation of joints exhibiting strong and reproducible critical currents [8]. A solder alloy must also have low resistivity to minimize the total resistance of the soldered joint [3, 10, 11]. The mechanical behaviour of the solder also plays a critical role in joint strength, with the alloy composition being the most important factor governing mechanical properties [19]. The solder microstructure and the quality of the interface between the solder and the tape strongly influence the final joint performance [16, 20–22]. No holes, gaps, or cracks must be present at the interface of the solder and tape substrates in a salient solder joint [16]. The solder microstructure that develops during solidification relies on several dependent factors, including cooling rate, solder volume, and solder composition. The solder composition plays an important role in controlling the solder solidification behavior, including the formation and growth of primary intermetallic compounds (IMCs) [23, 24].

A number of Pb-free solders, including eutectic InSn [3, 15], SnBi [25–28], InBi [15, 29, 30] and Sn-Ag-Cu [4, 17, 31, 32] solders have been reported in the literature for joining ReBCO tapes. However, Sn-Ag-Cu, specifically SAC305, has a relatively high melting temperature and may damage the delicate YBCO layer. In contrast, the $In_{52}Sn_{48}$ alloy offers low melting point (118 °C), low resistivity, and relatively well-characterized thermal properties compared to other Pb-free options [3]. Nonetheless, research on InSn solder alloys remains limited, and some basic properties, such as mechanical strength of the joints and interfacial microstructure, have not been well reported. Despite ongoing attempts to develop the ReBCO joint quality, there is a limited systematic comparison of binary versus ternary low-melting-point Pb-free alloys for joining commercial ReBCO tapes. Moreover, present studies rarely integrate electrical, microstructural, and mechanical evaluation under identical processing conditions. Addressing this gap is the primary aim of this work. In this paper, we investigate the potential of low-temperature Pb-free solders, including binary In-Sn, In-Bi, Sn-Bi, and ternary Sn-In-Bi alloys, regarded as potential candidates for cryogenic applications [16, 33, 34], to develop low-resistance, mechanically robust joints between ReBCO tapes. We report comprehensive microstructural analysis along with electrical and mechanical properties of the joints to identify the optimal Pb-free solders among these candidates for ReBCO magnet developments.

2 Methodology

Table 1 shows the Pb-free solder compositions fabricated in this study for joining ReBCO tapes. All alloy compositions reported in this work are expressed in weight%. The eutectics $In_{52}Sn_{48}$, $In_{66}Bi_{34}$, and $Sn_{42}Bi_{58}$ as binary solder candidates and $In_{50}Sn_{15}Bi_{35}$ as a ternary eutectic composition of In-Sn-Bi solder were selected for joining ReBCO tapes with melting points below 200 °C. These low-temperature alloys were fabricated from pure Sn, In, and Bi pellets (with high purity above 99.9%) by weighing the pellets and melting the mixture at temperatures up to 300 °C in a cylindrical alumina crucible on a hot plate.

The ReBCO tapes used in this work are commercial 12 mm-width YBCO tapes (FFJ-7053), with a nominal critical current (I_c) of 498 A at 77 K and under self-field conditions, manufactured by Faraday Factory Japan. This YBCO tape has been fabricated by surrounding silver and copper stabilizers, which are added via magnetron sputtering and electroplating to provide thermal and electrical stability. To fabricate the joint, the YBCO tapes were first prepared by gently polishing and subsequently cleaning using ethanol and acetone. Then, they were wetted by a thin film of rosin soldering flux. The prepared tapes were subsequently inserted into a molten solder bath for a few moments at a temperature determined by the melting points listed in Table 1. In the next step, a 1.5 cm overlap configuration was placed on a hot plate under a one kg load, and the joint was then fabricated at a cooling rate of approximately 12 °C/min. The joining conditions were kept identical for all samples to ensure a reliable comparison of the solder compositions and their resulting joint performance. The morphology of the joints was characterized using a

Table 1 Solder type compositions fabricated in this study, along with their melting temperature

Solder composition	$In_{52}Sn_{48}$	$In_{66}Bi_{34}$	$Sn_{42}Bi_{58}$	$In_{50}Sn_{15}Bi_{35}$
Melting point (°C)	118 (15, 35)	72 (15, 36)	138 (37)	55 (16)

Zeiss scanning electron microscope (SEM) operating at an accelerating voltage of 20 kV, and equipped with an Oxford Instruments energy-dispersive X-ray spectroscopy (EDS) system, and the data were analyzed using Aztec software. The joint resistance was measured using the standard four-probe technique at 77 K in a liquid nitrogen bath, under self-field conditions, with a DC power supply. An Instron universal testing machine, equipped with a 50 kN load cell, 2 kN pneumatic grips, and serrated-faced jaws operated at 2 bar pressure, at a crosshead displacement speed of 1 mm/min, was also employed to evaluate the sample's mechanical strength at room temperature. All samples were tested under identical experimental conditions, including the same gauge length.

3 Results and Discussion

3.1 Joint Electrical Resistance

The joint resistance can be determined from the slope of the V-I curve in the linear region. Fig. 1 shows the V-I measurement data for the joints fabricated in this study. As shown in this graph, the joints exhibit an ohmic behavior at currents below I_c, and the voltage increases linearly with current. In this regard, the joint resistance was determined by fitting a straight line to the data obtained from four-probe measurements on the samples at 77 K under self-field conditions. Based on the slope of each line, the resistance value for the joint was determined as 25.98 nΩ for $In_{66}Bi_{34}$, 65.32 nΩ for $Sn_{42}Bi_{58}$, 67.02 nΩ for $In_{52}Sn_{48}$, and 101.32 nΩ for $In_{50}Sn_{15}Bi_{35}$, and these values are presented beside the fitted lines in Fig. 1. The results show that the joints fabricated with the binary solders had lower resistance compared to the joint made using the ternary $In_{50}Sn_{15}Bi_{35}$ solder. Among binary solders, the joint made by $In_{66}Bi_{34}$ alloy exhibits the lowest electrical resistance, and the $In_{52}Sn_{48}$ shows the highest joint resistance. To understand the resistance variations between these joints, microstructural analysis was carried out (presented in the next section) to investigate the microstructure of the solder and the tape/solder interface.

3.2 Joint Microstructural Characterization

3.2.1 $In_{66}Bi_{34}$

Figure 2(a) exhibits the backscattered electron (BSE) image of the eutectic $In_{66}Bi_{34}$ joint cross-section, illustrating the formation of a uniform 30-µm solder layer and well-defined interfaces between the solder and the copper stabilizers. Fig. 2(b-g) presents a higher-magnification BSE/SEM image of the solder/tape interface, together with the corresponding EDS elemental maps and line-scan analysis. The EDS data reveal the presence of a thin, continuous interfacial layer containing Cu and In, shown in Fig. 2(b) and (c). The line-scan analysis across the interface layer, presented in Fig. 2(g), confirms a composition corresponding to $CuIn_2$ intermetallic compound at this interface, and shows that Bi did not participate in the interfacial reaction. This IMC has also been observed in other reports [38].

To characterize the solder microstructure in the joint region, higher-magnification analyses were conducted within the solder area. As shown in Fig. 2(h) and the elemental maps in Fig. 2(i-k), the solder solidifies into a two-phase microstructure expected for the InBi eutectic composition. The compositions of these phases have been obtained by EDS analyses, including point analysis, to be a light $BiIn_2$ intermetallic compound and a dark In-rich phase. In fact,

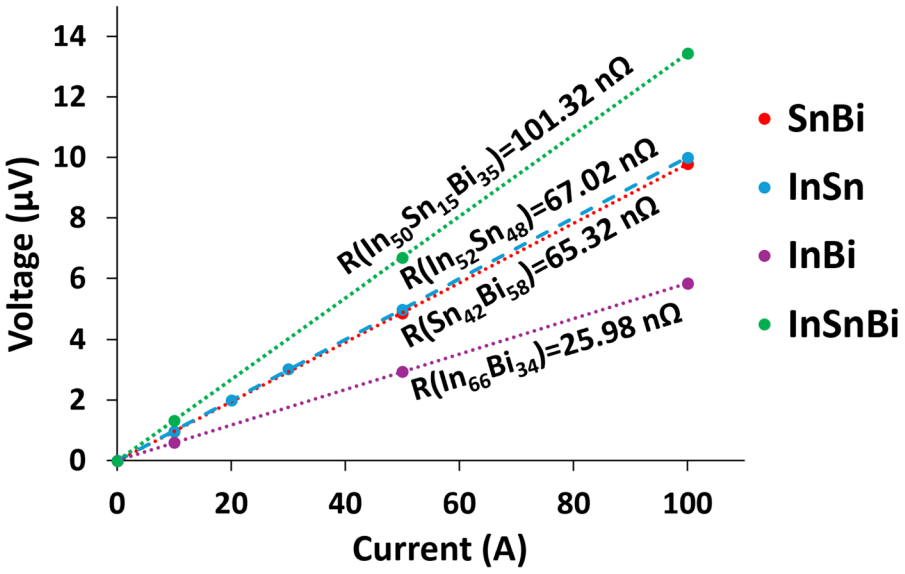

Fig. 1 V-I data of the joints obtained through the four-probe measurement at 77 K and under self-field conditions, along with the resistance values for the fabricated joints

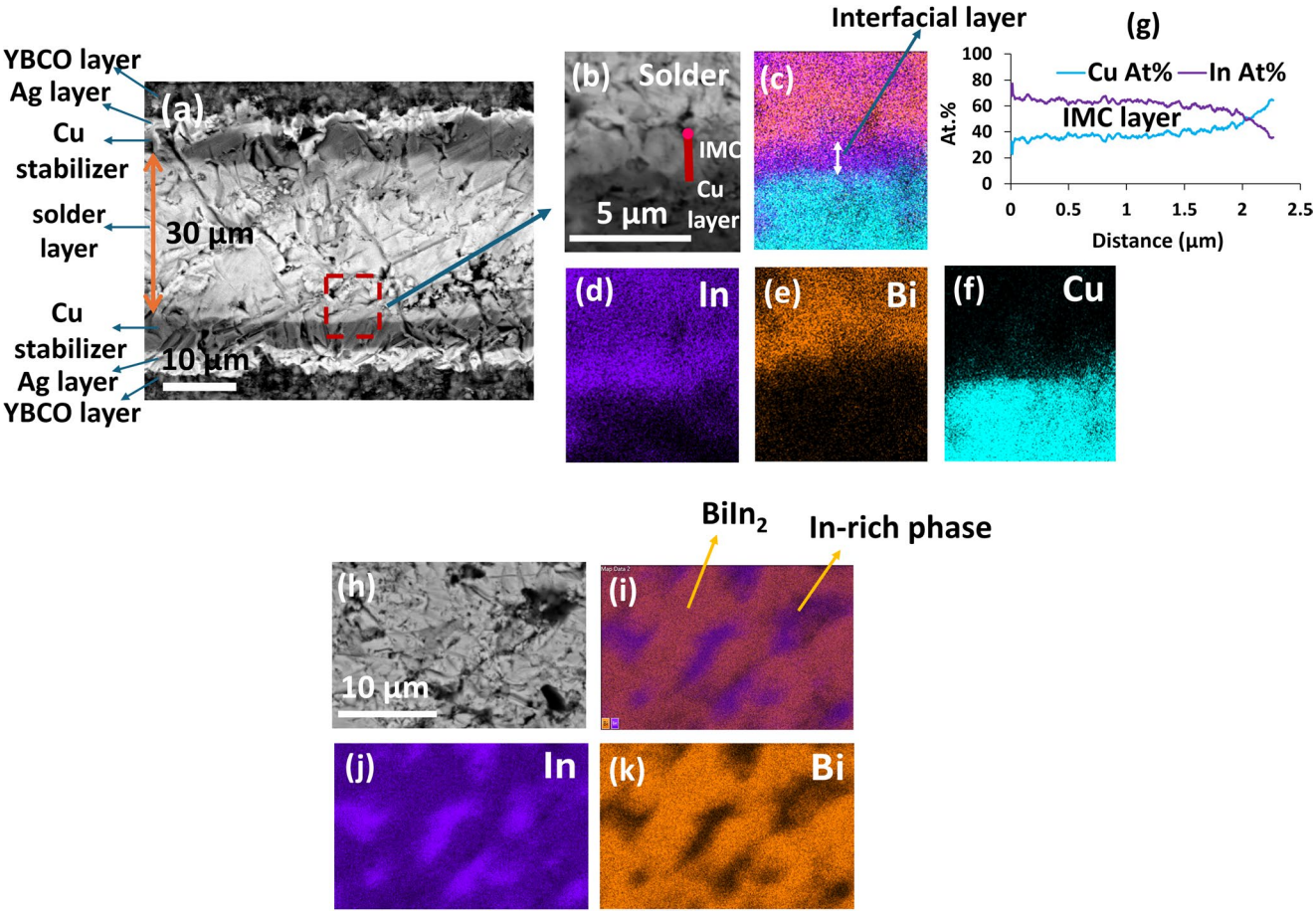

Fig. 2 **a** BSE/SEM micrograph of the $In_{66}Bi_{34}$ joint cross section, **b** BSE/SEM image of the joint with higher magnification to show the solder/tape interface, **c** merged elemental map of the solder/tape interface, **d-f** In, Bi and Cu elemental maps, **g** line-scan analysis of solder/Cu layer interface, **h** BSE/SEM image of the solder area, **i** merged elemental map of the solder area, **j** and **k** In and Bi elemental maps

upon cooling, the eutectic reaction occurring at 72 °C forms the two equilibrium eutectic phases of α and $BiIn_2$ through the reaction of Liquid → α + $BiIn_2$, and with further cooling, a eutectoid reaction of α → In-rich + $BiIn_2$ happens at 46.6 °C, and the solder microstructure includes $BiIn_2$ and In-rich phases at room temperature [36]. Hence, the resulting microstructure comprises an In-rich phase, and the $BiIn_2$ intermetallic compound with a relatively higher volume fraction.

3.2.2 $In_{52}Sn_{48}$

Figure 3(a) presents the BSE/SEM micrograph of the $In_{52}Sn_{48}$ joint cross-section, revealing a homogeneous 30-µm-thick solder layer and a continuous solder/interface structure. Fig. 3 (b) depicts that a few-micron-thick interfacial layer forms at the solder/Cu interface in the eutectic InSn joint. To more closely evaluate this region, showing the interface between the solder and Cu layer of the tape, a high-magnification EDS line scan was performed across the interface. The EDS results confirm the formation of $Cu_2(In,Sn)$ as the intermetallic compound at the solder/Cu interface boundary. Among the possible interfacial phases, $Cu_2(In,Sn)$ is commonly reported as the primary intermetallic compound that forms at soldering temperatures below 200 °C at the solder/Cu layer interface [39, 40], in agreement with the observations in this study.

The accompanying SEM/EDS analysis of the solder area, presented in Fig. 3(d-g), indicates that a two-phase microstructure composed of In-rich (β) and Sn-rich (γ) phases formed during the solidification of the eutectic InSn alloy. The presence of these phases is consistent with the In-Sn phase diagram and previous reports on eutectic solidification in this binary system [21, 35, 41].

3.2.3 $Sn_{42}Bi_{58}$

Figure 4 (a) shows the BSE/SEM image of the solder joint fabricated using $Sn_{42}Bi_{58}$ solder, representing a uniform 40-µm-thick solder structure bounded on both sides by thin and continuous interfacial layers. To evaluate the solder/Cu interface, a higher-magnification BSE/SEM image and

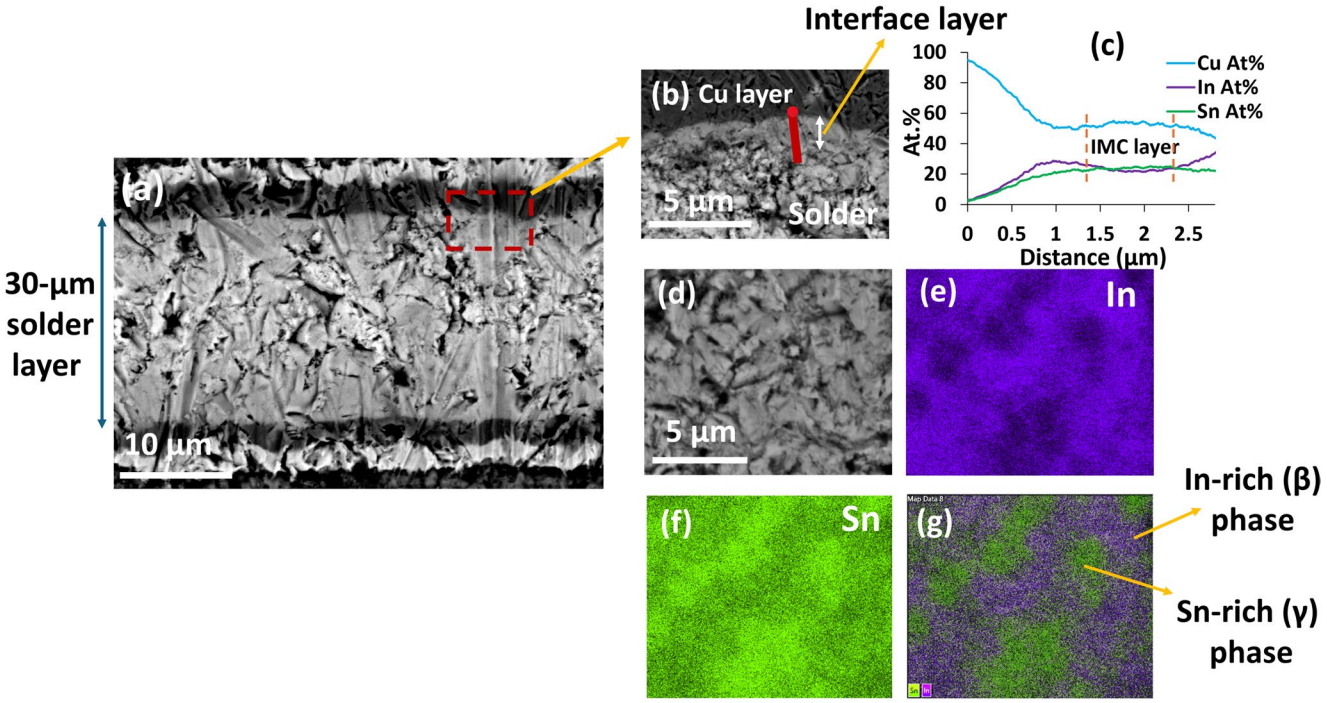

Fig. 3 **a** BSE/SEM micrograph of the $In_{52}Sn_{48}$ joint, **b** BSE/SEM image of the joint with higher magnification to show the solder/tape interface, **c** line-scan analysis of solder/Cu layer interface, **d** BSE/SEM image of the solder area, **e** and **f** In and Sn elemental maps, **g** merged elemental map

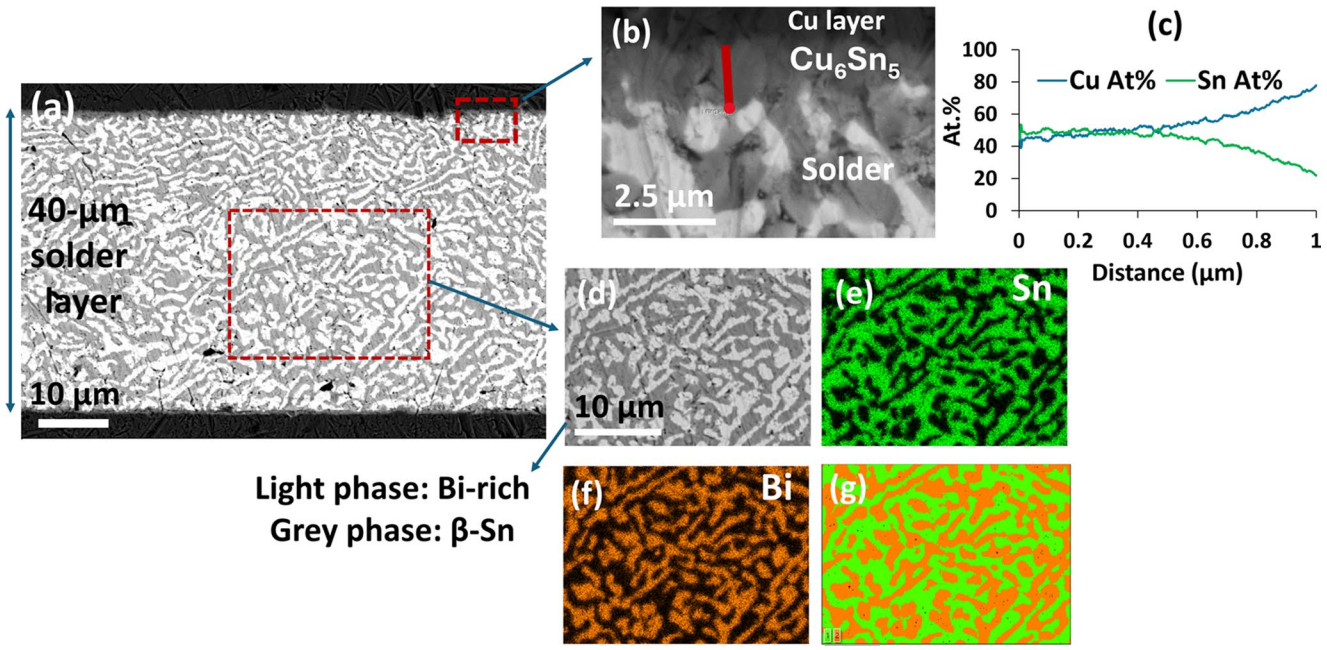

Fig. 4 **a** BSE/SEM micrograph of the $Sn_{42}Bi_{58}$ joint, **b** BSE/SEM image of the joint with higher magnification to show the solder/tape interface, **c** line-scan analysis of solder/Cu layer interface, **d** BSE/SEM image of the solder area, **e** and **f** Sn and Bi elemental maps, **g** merged phase map

corresponding EDS line-scan analysis were acquired, shown in Fig. 4(b) and (c), respectively. The results of line-scan and point analyses depict the formation of a thin interfacial IMC layer composed of Cu and Sn, with a composition identified as Cu_6Sn_5, which is consistent with earlier findings reported in the literature [37]. EDS elemental and phase maps of the solder region (Fig. 4 (d-g)) show a typical lamellar/striped two-phase eutectic microstructure, consisting of alternating grey β-Sn and light Bi-rich phases. This morphology results from the instantaneous phase separation during eutectic

solidification, consistent with previous reports [37]. In fact, upon cooling, a eutectic reaction directly occurs to form the two equilibrium phases once the temperature reaches 138 °C. According to the Sn-Bi binary phase diagram [37, 42], the β-Sn phase is a solid solution rich in Bi with the solubility limit of 21 wt%, occurring at eutectic temperature, while there is almost no solubility for Sn in Bi.

3.2.4 $In_{50}Sn_{15}Bi_{35}$

Figure 5(a) presents the BSE/SEM image of the $In_{50}Sn_{15}Bi_{35}$ joint cross-section, with a 35-µm-thick solder layer. Fig. 5(b) and (c) show the BSE/SEM image and EDS line-scan data obtained across the interface between the solder and the Cu stabilizer of the tape for this ternary joint. The EDS analysis indicates the formation of a thin and uniform interfacial layer composed of Cu, Sn, and In, with a composition identified as Cu_3SnIn. The elemental maps of the solder region, shown in Fig. 5 (d-h), confirm the ternary eutectic composition of $In_{50}Sn_{15}Bi_{35}$ in the Sn-In-Bi system, showing clear elemental segregation of In, Sn, and Bi. The microstructure consists of three distinct phases formed through the eutectic reaction of Liquid → γ + β + $BiIn_2$. The $BiIn_2$ phase appears as the dominant, light matrix phase, within which darker γ (Sn-rich) and β (In-rich) phases are distributed in about similar proportions. The same microstructural features have been reported previously for this ternary eutectic composition in the In-Sn-Bi system [16, 42].

3.3 Joint Mechanical Properties at Room Temperature

The mechanical behavior of the soldered joint samples was evaluated using axial tensile testing to assess the influence of solder type on their strength. In this regard, stress-strain curves, shown in Fig. 6 (a), were obtained by calculating the stress as the applied force divided by the tape's cross-sectional area (tape width × tape thickness), and the strain from the crosshead displacement of the testing machine divided by the initial gauge length. Under axial loading, the applied tensile force along the tape length is transferred as shear stress across the overlap region of the joint. Accordingly, the joint tensile strength at failure can be estimated by dividing the fracture load by the joint cross-sectional area (overlap length × joint width), and the results are presented in Fig. 6 (b). Notably, all samples failed in the tape region rather than within the joint area under the applied loading conditions at room temperature. This indicates that the joints possess higher mechanical stability than the original tape and were capable of sustaining at least $\tau_{\text{failure at the joint}}$. Because failure did not initiate within the solder or at the solder/tape interface, it can be concluded that the joints produced in this study are mechanically robust, and the joint itself was not the limiting factor in tensile performance. It should be mentioned that the measured tensile values of engineering stress-strain curves correspond to the overall tensile capacity of the assembly rather than the joint strength and were used for comparative evaluation of the samples' mechanical performance under identical

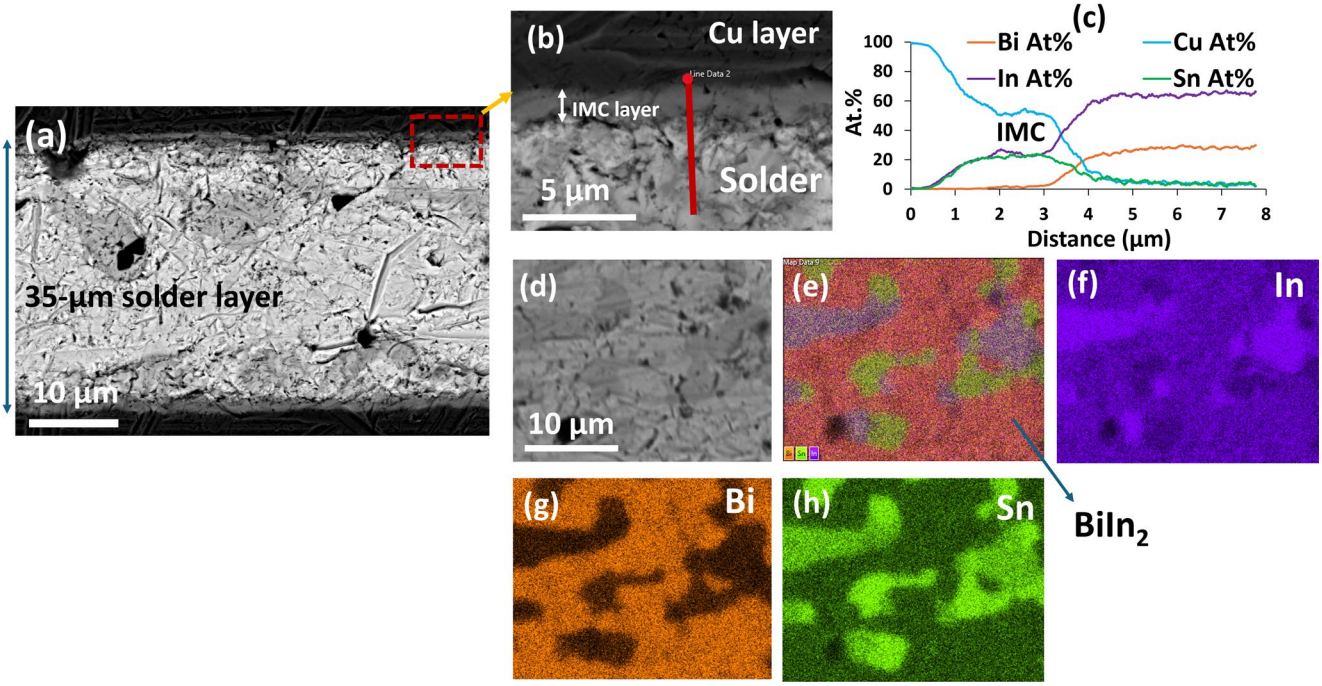

Fig. 5 **a** BSE/SEM image of the $In_{50}Sn_{15}Bi_{35}$ solder joint, **b** BSE/SEM image of the joint with higher magnification to show the solder/tape interface, **c** line-scan analysis of solder/Cu layer interface, **d** BSE/SEM image of the solder area, **e** merged elemental map, **f-h** In, Bi and Sn elemental maps

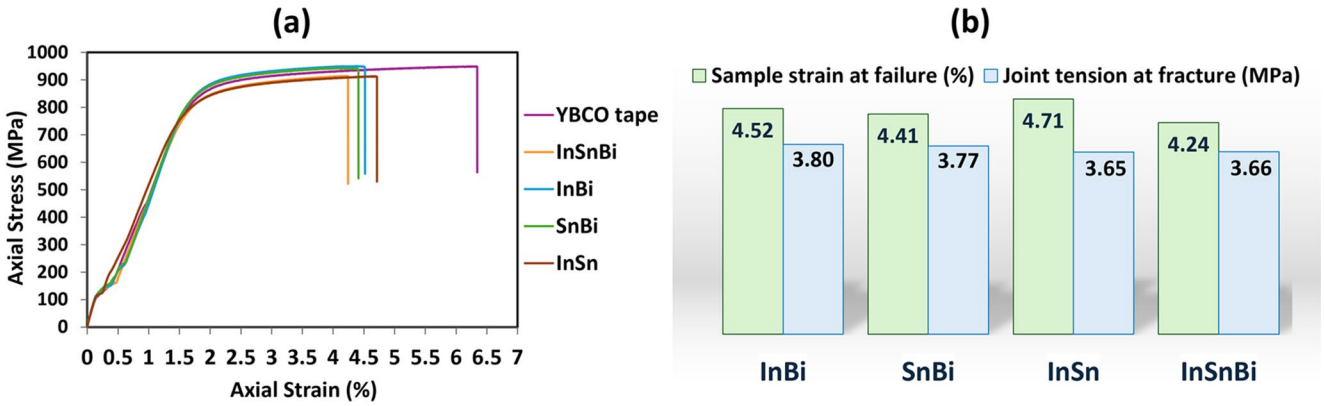

Fig. 6 **a** Engineering stress-strain curves of all the specimens, along with **b** bar chart of the joints' tension values and samples' strain percentages at failure

testing conditions. Differences in failure stress reflect overall sample tensile strength, and it should not be interpreted as direct differences in intrinsic joint strength. A comparison of the measured tensile response with previously reported data for soldered YBCO joints in the literature shows that the obtained fracture loads and overall mechanical behavior are consistent with published results, when differences in testing conditions, including strain measurement methodology, are taken into account. In particular, studies employing extensometers directly attached to the specimen typically report lower strain values compared to those based on crosshead displacement measurements [6, 43, 44].

3.4 Discussion

This study focuses on low-melting, Pb-free eutectic alloys specifically selected to minimize the thermal impact on the tape during joining. The SEM/EDS analyses of the joints' cross-sections showed no damage to the susceptible YBCO layers of the tapes, confirming the suitability of the joining process. During soldering with a Cu substrate, interfacial reactions occurring at the solder/Cu interface and within the solder matrix form an IMC layer, which is essential for metallurgical bonding [37]. The nucleation and growth of this IMC layer between the solder and the tape play a critical role in determining the overall reliability of the joint. Proper IMC formation indicates good metallurgical bonding between the solder and tape [45]. Moreover, the presence of a thin, continuous, and uniform IMC layer between the solder and the copper stabilizer of the tape can enhance the joint's mechanical properties [3, 12, 26, 46–48]. However, IMCs are inherently hard and brittle, which can compromise the integrity of the solder joint [45, 49]. Excessive growth of brittle IMCs at the Cu/solder interface weakens interfacial bonding, reduces the solder joint's mechanical strength and reliability, and shortens the joint's lifetime due to their fragility and tendency to form structural defects, particularly under impact loading [12, 31, 50]. Microstructural analysis of the fabricated joints in this study showed that all IMC layers formed at the solder/tape interfaces were thin.

The solder microstructure after solidification is influenced by multiple factors, including solder volume, composition, joining duration and the cooling rate during joint fabrication. Hence, the solder type is one of the key elements that determines the composition of phases formed in the solder and at the solder/tape interface. As the joining condition was the same for all the fabricated joints, the solder composition plays the main role in determining the solder solidification behaviour and the resultant phases. While the resistance of the joint is affected by the resistance of each phase presented in the joint region, the presence of three distinct phases, compared to two in the binary joints, may explain the higher total resistance of the $In_{50}Sn_{15}Bi_{35}$ joint. This means that increasing the number of phases in the solder layer introduces additional scattering sites for current due to the extra phases and interphase boundaries in the joint region. Moreover, in the ternary $In_{50}Sn_{15}Bi_{35}$ solder, the primary matrix phase is $BiIn_2$ (as shown in Fig. 5), an intermetallic compound with inherently higher electrical resistivity. Together, the increased number of scattering centers and the dominance of a resistive IMC matrix seem to be the reasons for the higher joint resistance observed in this ternary solder compared to the binary solder joints in this study. Furthermore, a higher density of interphase boundaries in the joint region can further increase the overall electrical resistance [51]. Examining the microstructure of the solder in the joint area shows that all solders investigated in this study exhibit a similar microstructural scale (approximately 5 μm). This similarity results from the consistent joining conditions used for all joints, including a similar cooling rate. Consequently, the interphase boundary density does not appear to be a major factor governing the differences in electrical resistance among the solders examined in this work.

Table 2 summarizes the microstructural, electrical and mechanical characteristics of the joints fabricated with

Table 2 Summary of the features and properties obtained for the fabricated joints in this study

Solder composition	$In_{66}Bi_{34}$	$In_{52}Sn_{48}$	$Sn_{42}Bi_{58}$	$In_{50}Sn_{15}Bi_{35}$
Solder phases	In-rich +$BiIn_2$	β(In-rich) + γ(Sn-rich)	β(Sn-rich) + Bi-rich	γ (Sn-rich) +β (In-rich) +$BiIn_2$
Solder/tape Interface phases	$CuIn_2$	Cu_2InSn	Cu_6Sn_5	Cu_3SnIn
Joint resistance (nΩ)	25.98	67.02	65.32	101.32
Joint tension at failure (MPa)	3.80	3.65	3.77	3.66

different Pb-free solders in this work. All the joints produced in this study demonstrated high mechanical strength, and fracture did not initiate in the solder region or at the solder/tape interfaces. Possible reasons for the good mechanical strength of the fabricated joints are the formation of a thin IMC layer between the Cu stabilizer (from the YBCO tape) and the solder, as well as effective wetting, as revealed by the microstructural analysis. The IMC layers formed in each joint are listed in Table 2. Their presence indicates that diffusion occurs at the interface, and the tape and solder are chemically bonded, creating a high mechanical strength. Moreover, interfacial chemical diffusion and IMC formation at the interface prevent the development of holes and cracks, which is critical for both mechanical robustness and electrical performance. Although the presence of an IMC layer at the interface provides several benefits, one downside would be the additional resistance it introduces to supercurrent flow through the joint region, as the current must pass through an additional layer. Thus, variations in the IMCs formed at the solder/tape interfaces may also contribute to differences in the total joint resistance values measured using the 4-probe technique.

4 Conclusion

This work has studied four low-temperature Pb-free eutectic solders, the binary $In_{66}Bi_{34}$, $In_{52}Sn_{48}$, $Sn_{42}Bi_{58}$, and the ternary $In_{50}Sn_{15}Bi_{35}$, for fabricating lap joints between FFJ YBCO tapes, evaluating the joint microstructure, electrical resistance at 77 K, and room-temperature tensile strength. The microstructure of soldered lap joints after solidification, within the solder and at the solder/tape interface, plays a vital role in determining the final properties of YBCO joints. Solder composition was found to be the primary factor controlling both the solder microstructure and the interfacial phases, which, in turn, govern the joint's electrical and mechanical performance. Overall, the binary eutectic solders produced simpler two-phase solder microstructures and exhibited lower joint resistance compared to the ternary $In_{50}Sn_{15}Bi_{35}$ solder. Among the alloys examined, the eutectic $In_{66}Bi_{34}$ joint exhibited the best overall performance, combining a uniform solder microstructure, relatively low electrical resistance at 77 K, and good mechanical integrity, making it a promising Pb-free alternative to conventional Pb-Sn solders for superconducting applications. Notably, all joints failed within the tape rather than the soldered region under axial tension at room temperature, indicating that the soldered joints were mechanically robust under the tested conditions. Electrical and microstructural evidence also indicates that reducing the number and volume fraction of high-resistivity IMC phases in the solder matrix, as well as limiting excessive interfacial IMC growth, is key to minimizing joint resistance. All in all, the results demonstrate that Pb-free binary eutectic alloys, particularly $In_{66}Bi_{34}$, are viable replacements for Pb-Sn solders, meeting the electrical and mechanical requirements for ReBCO joints in high-field magnet applications.

Authors' Contributions N.G.: Conducted the experiments, wrote the main manuscript, prepared figures, data analysis, discussion and review. K.B.: Technical support on electrical resistance measurements, and advice on electrical data analysis. A.M.: Supplied the YBCO tapes, and technical advice on the tape properties. M.A.: Critical manuscript review. T.M.: Critical manuscript review, advice on data analysis, and add discussion.

Data Availability All data supporting the findings of this study are available within the paper.

Declarations

Competing interests The authors declare no competing interests.

References

1. Liao, T., Wang, W., Chen, Z., Guan, M.: Numerical study on mechanical behavior and electromechanical properties of solder-jointed REBCO-coated conductors. Materials. **17**(11), 2517 (2024). https://doi.org/10.3390/ma17112517
2. Whyte, D.G., Minervini, J., LaBombard, B., Marmar, E., Bromberg, L., Greenwald, M.: Smaller & Sooner: exploiting high magnetic fields from new superconductors for a more attractive fusion energy development path. J. Fusion Energy. **35**(1), (2016). https://doi.org/10.1007/s10894-015-0050-1

3. Tsui, Y., Surrey, E., Hampshire, D.: Soldered joints—an essential component of demountable high temperature superconducting fusion magnets. Supercond. Sci. Technol. **29**(7), 075005 (2016). https://doi.org/10.1088/0953-2048/29/7/075005
4. Skarba, M., Pekarčíková, M., Frolek, L., Cuninková, E., Necpal, M.: Thermal cycling of (Re)BCO-based superconducting tapes joined by lead-free solders. Materials. **14**(4), (2021). https://doi.org/10.3390/ma14041052
5. Preuss, A., Fietz, W.H., Immel, F., Kauffmann-Weiss, S., Wolf, M.J.: Critical Current degradation of coated conductors under soldering conditions. IEEE Trans. Appl. Supercond. **28**(4), (2018). https://doi.org/10.1109/TASC.2018.2804094
6. Huang, D., Gu, H., Dong, Z., Shang, H., Xu, W., Li, T., et al.: Study on electromechanical properties of solder jointed YBCO coated conductors with etched copper stabilizer under axial tension. IEEE Trans. Appl. Supercond. **30**(1), (2020). https://doi.org/10.1109/TASC.2019.2926261
7. Huang, Z., Tan, Y., He, R., Xie, Y., Wang, G., Wei, J., et al.: Study on the electrical performances of soldered joints between HTS coated-conductors. Cryogenics (Guildf). **122**, 103422 (2022). https://doi.org/10.1016/j.cryogenics.2022.103422
8. Kim, Y., Bascunan, J., Lecrevisse, T., Hahn, S., Voccio, J., Park, D.K., et al.: YBCO and Bi2223 coils for high field LTS/HTS NMR magnets: HTS-HTS joint resistivity. IEEE Trans. Appl. Supercon. **23**(3), (2013). https://doi.org/10.1109/TASC.2013.2243195
9. Bagrets, N., Celentano, G., Augieri, A., Nast, R., Weiss, K.P.: Investigation of soldered REBCO tape-copper joints for superconducting applications. IEEE Trans. Appl. Supercon. **26**(4), (2016). https://doi.org/10.1109/TASC.2016.2519928
10. Tsui, Y., Mahmoud, R., Surrey, E., Hampshire, D.: Superconducting and mechanical properties of low-temperature solders for joints. IEEE Trans. Appl. Supercon. **26**(3), (2016). https://doi.org/10.1109/TASC.2016.2536806
11. Amin, N.A.A.M., Shnawah, D.A., Said, S.M., Sabri, M.F.M., Arof, H.: Effect of Ag content and the minor alloying element Fe on the electrical resistivity of Sn-Ag-Cu solder alloy. J. Alloys Compd. 599 (2014). https://doi.org/10.1016/j.jallcom.2014.02.100
12. Zhang, Y., Duckworth, R.C., Ha, T.T., Gouge, M.J.: Solderability study of RABiTS-based YBCO coated conductors. Physica C: Supercon. Appl. **471**, 15–16 (2011). https://doi.org/10.1016/j.physc.2011.03.009
13. Lu, J., Han, K., Sheppard, W.R., Viouchkov, Y.L., Pickard, K.W., Markiewicz, W.D.: Lap joint resistance of YBCO coated conductors. IEEE Trans. Appl. Supercon. **21**(3 PART 3), (2011). https://doi.org/10.1109/TASC.2010.2091934
14. Baldan, C.A., Oliveira, U.R., Bernardes, A.A., Oliveira, V.P., Shigue, C.Y., Ruppert, E.: Electrical and superconducting properties in lap joints for YBCO tapes. J. Supercond. Nov. Magn. **26**(5), (2013). https://doi.org/10.1007/s10948-012-1905-6
15. Zhang, S., Li, F., Yang, G., Xu, S., Han, Z., Fan, Z., et al.: Enhanced electrical and mechanical performances of soldered joint between copper stabilized REBCO superconducting tapes. IEEE Trans. Appl. Supercon. **29**(5), (2019). https://doi.org/10.1109/TASC.2019.2896459
16. Mousavi, T., Aksoy, C., Grovenor, C., Speller, S.: Phase evolution of superconducting Sn-In-Bi solder alloys. IEEE Trans. Appl. Supercond. **26**(3), (2016). https://doi.org/10.1109/TASC.2016.2514843
17. Drienovsky, M., Michalcová, E., Pekarčíková, M., Palcut, M., Frolek, L., Gogola, P., et al.: Induction soldering of coated conductor high-temperature superconducting tapes with lead-free solder alloys. IEEE Trans. Appl. Supercond. **28**(4), (2018). https://doi.org/10.1109/TASC.2018.2805102
18. Chen, Y., Fu, L., Wang, W., Xu, J., Ni, F., Lin, G., et al.: A generalized model of HTS-HTS joint resistance for superconducting magnets. IEEE Trans. Appl. Supercon. **34**(8), 1–4 (2024). https://doi.org/10.1109/TASC.2024.3391789
19. Zhao, M., Zhang, L., Liu, Z.Q., Xiong, M.Y., Sun, L.: Structure and properties of Sn-Cu lead-free solders in electronics packaging. Sci. Technol. Adv. Mater. (2019). https://doi.org/10.1080/14686996.2019.1591168
20. Brittles, G.D., Mousavi, T., Grovenor, C.R.M., Aksoy, C., Speller, S.C.: Persistent current joints between technological superconductors. Supercond. Sci. Technol. (2015). https://doi.org/10.1088/0953-2048/28/9/093001
21. Goodarzi, N., Berger, K., Molodyk, A., Ainslie, M., Mousavi, T.: Development of Ag-Added InSn solders for ReBCO joints. IEEE Trans. Appl. Supercond. **36**(5), 1–5 (2026). https://doi.org/10.1109/TASC.2025.3646983
22. Goodarzi, N., Berger, K., Molodyk, A., Ainslie, M., Mousavi, T.: Impact of Ga addition to In Sn solder on ReBCO joint performance. IEEE Trans. Appl. Supercond. (2026)
23. Kotadia, H.R., Howes, P.D., Mannan, S.H.: A review: On the development of low melting temperature Pb-free solders. Microelectron. Reliab. (2014). https://doi.org/10.1016/j.microrel.2014.02.025
24. Mueller, M., Wiese, S., Roellig, M., Wolter, K.J.: Effect of composition and cooling rate on the microstructure of SnAgCu-solder joints. Proc. – Electron. Compon. Technol. Conf. (2007). https://doi.org/10.1109/ECTC.2007.374006
25. Mei, Z., Morris, J.W.: Characterization of eutectic Sn-Bi solder joints. J. Electron. Mater. **21**(6), (1992). https://doi.org/10.1007/BF02655427
26. Zheng, J., Ma, H., He, R., Lu, Y., Song, H., Cui, C., et al.: Low-resistance and strong-adhesion soldering of second-generation high-temperature superconductor tapes within a short time. IEEE Trans. Appl. Supercon. **27**(5), (2017). https://doi.org/10.1109/TASC.2017.2698203
27. Zhang, H., Ma, G., Li, X., Peng, J., Xu, Z., Gong, T., et al.: A simple and effective process to join coated super- conductors at a low resistance. Xiyou Jinshu Cailiao Yu Gongcheng/Rare Metal Materials and Engineering. **47**(3), (2018). https://doi.org/10.1016/s1875-5372(18)30103-6
28. Lee, N.C.: Lead-free soldering - where the world is going. Adv. Microelectron. **26**(5), (1999)
29. Park, D.K., Ahn, M.C., Kim, H.M., Lee, H.G., Chang, K.S., Lee, S.J., et al.: Analysis of a joint method between superconducting YBCO coated conductors. IEEE Trans. Appl. Supercond. (2007). https://doi.org/10.1109/TASC.2007.899590
30. Shin, H.S., Dedicatoria, M.J., Oh, S.S.: Critical current degradation behavior in lap-jointed coated conductor tapes with IBAD substrate under uniaxial tension. IEEE Trans. Appl. Supercond. (2010). https://doi.org/10.1109/TASC.2010.2042049
31. Michalcova, E., Gomory, F., Frolek, L., Drienovsky, M., Pekarcikova, M., Skarba, M., et al.: Joining of CC tapes with lead-free solders. IEEE Trans. Appl. Supercond. **26**(3), (2016). https://doi.org/10.1109/TASC.2016.2539419
32. Liu, W., Zhang, X., Liu, Y., Zhou, J., Zhou, Y.: Lap joint characteristics of the YBCO coated conductors under axial tension. IEEE Trans. Appl. Supercond. **24**(6), (2014). https://doi.org/10.1109/TASC.2014.2332444
33. Jiye Zhou, X.F.T.S.D.M., KN.: Phase transformations and mechanical properties in In–Bi–Sn alloys as a result of low-temperature storage. Materials. (2024)
34. Mousavi, T., Aksoy, C., Grovenor, C.R.M., Speller, S.C.: Microstructure and superconducting properties of Sn-In and Sn-In-Bi alloys as Pb-free superconducting solders. Supercond. Sci. Technol. **29**(1), (2016). https://doi.org/10.1088/0953-2048/29/1/015012

35. Shu, Y., Ando, T., Yin, Q., Zhou, G., Gu, Z.: Phase diagram and structural evolution of tin/indium (Sn/In) nanosolder particles: From a non-equilibrium state to an equilibrium state. Nanoscale. **9**(34), (2017). https://doi.org/10.1039/c7nr01402c
36. Manasijević, I., Balanović, L., Grgurić, T.H., Minić, D., Gorgievski, M.: Study of microstructure and thermal properties of the low-melting Bi–In eutectic alloys. J. Therm. Anal. Calorim. (2019)
37. Wang, F., Huang, Y., Zhang, Z., Yan, C.: Interfacial reaction and mechanical properties of Sn-Bi solder joints. Materials. **10**(8), (2017). https://doi.org/10.3390/ma10080920
38. Tseng, T.H., Yang, C.H., Chiang, J.Y., Huang, J.J., Chen, C.H., Lin, S.K., et al.: Interfacial reactions of 68In–32Bi, 50In–50Bi and 33In–67Bi low melting alloys on Cu substrates. Mater Sci Eng : A. 759 (2019). https://doi.org/10.1016/j.msea.2019.05.074
39. Shang, P., Tian, F., Liu, Z.Q.: Identification and evolution of intermetallic compounds formed at the interface between In-48Sn and Cu during liquid soldering reactions. Metals (Basel). **14**(2), (2024). https://doi.org/10.3390/met14020139
40. Tian, F., Liu, Z.Q., Shang, P.J., Guo, J.: Phase identification on the intermetallic compound formed between eutectic SnIn solder and single crystalline Cu substrate. J. Alloys Compd. 591 (2014). https://doi.org/10.1016/j.jallcom.2013.12.257
41. Zhou, J., Tan, X.F., McDonald, S.D., Nogita, K.: Mechanical properties and microstructure of binary in-sn alloys for flexible low temperature electronic joints. Materials. **15**(23), (2022). https://doi.org/10.3390/ma15238321
42. Manasijević, I., Balanović, L., Grgurić, T.H., Minić, D., Gorgievski, M.: Study of microstructure and thermal properties of the low melting Bi-In-Sn eutectic alloys. Mater Res. **21**(6), (2018). https://doi.org/10.1590/1980-5373-MR-2018-0501
43. Su, X., Huang, Z., Liu, C., Zhang, X.: Controllable rectification on the irreversible strain limit of 2G HTS coated conductors. Supercond. Sci. Technol. **35**(1), (2022). https://doi.org/10.1088/1361-6668/ac39e9
44. Shin, H.S., Bautista, Z.: Establishing a test procedure for evaluating the electromechanical properties of practical REBCO coated conductor tapes by the uniaxial tension test at 77 K. Supercond. Sci. Technol. **32**(6), (2019). https://doi.org/10.1088/1361-6668/ab0309
45. Ramli, M.I.I., Salleh, M.A.A.M., Abdullah, M.M.A.B., Zaimi, N.S.M., Sandu, A.V., Vizureanu, P., et al.: Formation and growth of intermetallic compounds in lead-free solder joints: A review. Materials. (2022). https://doi.org/10.3390/ma15041451
46. Laurila, T., Vuorinen, V., Kivilahti, J.K.: Interfacial reactions between lead-free solders and common base materials. Mater. Sci. Eng. R Rep. (2005). https://doi.org/10.1016/j.mser.2005.03.001
47. Suh, J.O., Tu, K.N., Tamura, N.: Preferred orientation relationship between Cu6Sn5 scallop-type grains and Cu substrate in reactions between molten Sn-based solders and Cu. J. Appl. Phys. **102**(6), (2007). https://doi.org/10.1063/1.2776002
48. Bader, S.: Rapid formation of intermetallic compounds by interdiffusion in the Cu-Sn and Ni-Sn systems. Acta Metall. Mater. **43**(1), (1995). https://doi.org/10.1016/0956-7151(94)00224-6
49. Aurelio, G., Sommadossi, S.A., Cuello, G.J.: Crystal structure of Cu-Sn-in alloys around the η-phase field studied by neutron diffraction. J. Electron. Mater. **41**(11), (2012). https://doi.org/10.1007/s11664-012-2193-4
50. Ng, W.C.W., Sweatman, K., Akaiwa, T., Nishimura, T., Sato, M., Gourlay, C., et al.: Dissolution in service of the copper substrate of solder joints. In: Proceedings of the 2016 IEEE 18th electronics packaging technology conference, EPTC 2016 (2017). https://doi.org/10.1109/EPTC.2016.7861510
51. Bishara, H., Lee, S., Brink, T., Ghidelli, M., Dehm, G.: Understanding grain boundary electrical resistivity in cu: the effect of boundary structure. ACS Nano. **15**(10), (2021). https://doi.org/10.1021/acsnano.1c06367